BBA - Biomembranes 1860 (2018) 1783–1792

Contents lists available at ScienceDirect

BBA - Biomembranes

journal homepage: www.elsevier.com/locate/bbamem

A single mutation on the human amyloid polypeptide modulates fibril growth and affects the mechanism of amyloid-induced membrane damage

Anais R.F. Hoffmann[a], Manikam Sadasivam Saravanan[b], Olivier Lequin[a], J. Antoinette Killian[b], Lucie Khemtemourian[a,*]

[a] Sorbonne Université, Ecole Normale Supérieure, PSL University, CNRS, Laboratoire des Biomolécules, 4 place Jussieu, F-75005 Paris, France
[b] Department of Chemistry, Faculty of Science, Membrane Biochemistry and Biophysics, Bijvoet Center for Biomolecular Research, Padualaan 8, 3584 Utrecht, The Netherlands

ARTICLE INFO

Keywords:
Islet amyloid polypeptide
Amyloid-membrane interactions
Model membranes (LUV)
Aggregation kinetics
Membrane leakage
Type 2 diabetes mellitus

ABSTRACT

Amyloid fibril formation has been implicated in a wide range of human diseases and the interactions of amyloidogenic proteins with cell membranes are considered to be important in the aetiology of these pathologies. In type 2 diabetes mellitus (T2DM), the human islet amyloid polypeptide (hIAPP) forms amyloid fibrils which impair the functionality and viability of pancreatic β cells. The mechanisms of hIAPP cytotoxicity are linked to the ability of the peptide to self-aggregate and to interact with membranes. Previous studies have shown that the N-terminal part of hIAPP from residues 1 to 19 is the membrane binding domain. The non-amyloidogenic and nontoxic mouse IAPP differs from hIAPP by six residues out of 37, among which a single one, residue 18, lies in the membrane binding region. To gain more insight into hIAPP-membrane interactions we herein performed comprehensive biophysical studies on four analogues (H18R-IAPP, H18K-IAPP, H18E-IAPP and H18A-IAPP). Our data reveal that all peptides are able to insert efficiently in the membrane, indicating that residue 18 is not essential for hIAPP membrane binding and insertion. However, only wild-type hIAPP and H18K-IAPP are able to form fibrils at the membrane. Importantly, all peptides induce membrane damage; wild-type hIAPP and H18K-IAPP presumably cause membrane disruption mainly by fibril growth at the membrane, while for H18R-IAPP, H18E-IAPP and H18A-IAPP, membrane leakage is most likely due to high molecular weight oligomeric species. These results highlight the importance of the residue at position 18 in IAPP for modulating fibril formation at the membrane and the mechanisms of membrane leakage.

1. Introduction

Type 2 diabetes mellitus (T2DM) belongs to the family of protein misfolding diseases, which are characterized by abnormal accumulation of insoluble fibrillary protein aggregates [1,2]. These amyloid fibrils are usually found in the pancreatic islets of T2DM patients and are primarily composed of the 37-residue, human islet amyloid polypeptide (hIAPP, also known as amylin) [3,4]. Amyloid aggregation of hIAPP is not considered as the main cause of T2DM, but it is obviously a factor that impairs the functionality and viability of β cells and contributes to graft failure after islet transplantations [5–11]. hIAPP shares amino acid and structural similarity with calcitonin, calcitonin gene-related peptide and adrenomedullin [12,13]. The physiological function of hIAPP has not yet been completely determined; however it was shown that hIAPP plays a role in blood glucose homeostasis, in gastric emptying and other cellular processes such as bone metabolism, along with the related peptides calcitonin and calcitonin gene-related peptide [14].

Despite its clinical importance, the basis of hIAPP-induced cell toxicity is not entirely understood. It has been proposed that the toxicity of hIAPP is linked to its ability to perturb membranes and the details of hIAPP-membrane interaction have been the subject of several studies [15–20]. Many studies reported that the toxicity of amyloidogenic proteins, including hIAPP, is not linked to the insoluble fibrils themselves but rather to soluble oligomeric intermediates [21–23]. The existence of common structural features between amyloidogenic proteins was also established and thus a common cytotoxicity mechanism induced by small oligomeric species was proposed [24]. However, the existence of small oligomeric hIAPP species is more controversial and

Abbreviations: CD, circular dichroism; DOPC, 1,2-dioleoyl-sn-glycero-3-phosphocholine; DOPS, 1,2-dioleoyl-sn-glycero-3-phospho-L-serine; DMSO, dimethyl sulfoxide; HFIP, 1,1,1,3,3,3-hexafluoro-2-propanol; IAPP, Islet Amyloid Polypeptide; LUV, large unilamellar vesicle; T2DM, type 2 diabetes mellitus; TEM, transmission electron microscopy; NMR, Nuclear Magnetic Resonance; ThT, Thioflavin T

* Corresponding author at: CNRS, UMR 7203 Laboratoire des Biomolécules, F-75005 Paris, France.
E-mail address: lucie.khemtemourian@upmc.fr (L. Khemtemourian).

https://doi.org/10.1016/j.bbamem.2018.02.018
Received 22 December 2017; Received in revised form 19 February 2018; Accepted 20 February 2018
Available online 27 February 2018
0005-2736/

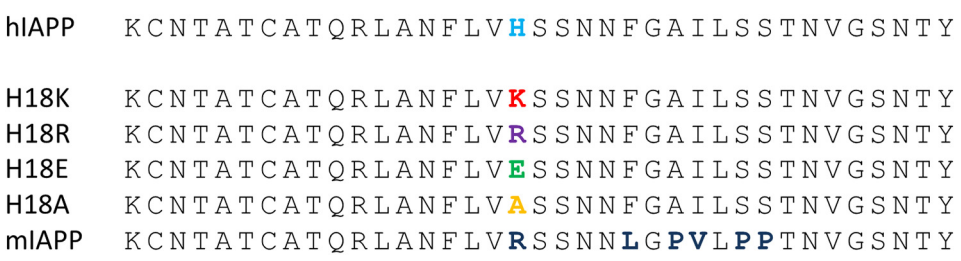

Fig. 1. Sequence of native human hIAPP (blue), the mutated peptides (H18K, red; H18R, purple; H18E, green; and H18A, yellow) and mouse mIAPP (dark blue). Each peptide contains a disulfide bond (Cys2 and Cys7) and an amidated C-terminus.

available data from the literature demonstrating the existence of IAPP oligomeric species are scarce [25–28]. Currently, the mechanism of hIAPP-membrane damage is still not clear and several hypotheses about the cause of hIAPP cytotoxicity have been postulated. Oligomeric pore-like structures of hIAPP have been proposed where monomeric hIAPP starts to aggregate into oligomers that interact with the membrane forming a pore [16,29,30]. In an alternative model, the membrane damage is a consequence of mechanical pressure induced by fibril growth at the surface of the membrane [31,32]. Although different hIAPP-membrane disruption mechanisms have been proposed, it is generally accepted that hIAPP interacts with cell membranes [31,33,34].

The amino acid sequence of hIAPP is shown in Fig. 1. hIAPP has an intramolecular disulfide bond between Cys2 and Cys7 and an amidated C terminus. Both the amidated C-terminus and the disulfide bridge are strongly conserved features throughout the mammalian species and both are necessary for the full biological activity of hIAPP [35,36]. Model membrane studies showed that hIAPP has a pronounced ability to interact and insert into lipid membranes [37,38] and that it adopts an alpha-helical conformation upon binding to vesicles containing negatively charged lipids [39,40]. More detailed structural information on the structure of hIAPP in the presence of model membranes was obtained by various biophysical approaches. Using electron paramagnetic resonance spectroscopy analysis the structure of hIAPP was determined in vesicles composed of zwitterionic and anionic lipids (PC:PS 20:80). The results indicated that the peptide adopts an α-helical structure between residue 9 to 22 and two less ordered segments were observed for the residues 1–8 and 23–37 [41]. Two NMR studies using sodium dodecyl sulfate (SDS) micelles provided additional support for this finding. The first study was carried out on non-amidated hIAPP at acidic pH and revealed three domains of hIAPP: an N-terminal region constrained by the disulfide bridge, an α-helical structure spanning residues 6–27 and an unfolded region from residues 28 to 37 [42]. The second NMR study, conducted on native amidated hIAPP at neutral pH, slightly differed from the previous one as the 7–28 helical structure was shown to be kinked by a turn segment around residues H18-S20 [43]. A recent molecular dynamics simulation in mixed lipidic membranes (PC:PS 70:30) showed helical content from residue 15 to 28 in agreement with NMR experimental work [44]. On the other hand, a high-resolution structural model of hIAPP obtained by NMR in a native lipid bilayer composed of zwitterionic and charged lipids (PC:PG) showed three antiparallel β strands (residues 8–12; 15–18 and 26–29) connected by flexible loops [45]. Thus, the conformational behavior of hIAPP is still a matter of some debate.

Further studies demonstrated that the N-terminal part of hIAPP (residues 1–19) i) mediates the insertion of the peptide into membranes, ii) does not damage membranes of relevant lipid composition [37,46,47] but iii) damages membranes when composed of anionic lipids only [48]. The mouse (mIAPP) or rat IAPP (rIAPP) differs from human IAPP by six residues out of 37 (Fig. 1). However, rIAPP and mIAPP do not form fibrils, are not toxic towards β-cells and rat and mice do not develop T2DM. It is interesting to note that there is only one amino acid difference in the 1–19 domain of IAPP, corresponding to His18 (for human IAPP) to Arg18 (mouse IAPP) substitution. A previous study on the 1–19 fragment of IAPP indicates that this domain disrupts the cellular membrane on pancreatic islets and allows the influx of calcium into the cell, suggesting an important role for His18 [49]. His18 is not only important for fibril formation and membrane interaction but also for binding of metal ions as it was shown in previous studies [50,51].

Recent investigations, using full-length hIAPP, proposed that residue 18 has a critical role in fibril formation and in mediating toxicity towards INS-1 β cells [33,49]. In addition, Martel and co-workers have simulated hIAPP-membrane insertion and calculated the depth of hIAPP-insertion using a mutated fragment of mIAPP (containing residues 1 to 20) where arginine 18 had been replaced by histidine 18. They reported that the residue 18 plays a crucial role in membrane insertion, underlining the importance of this residue in membrane affinity [20]. However, to our knowledge, no experimental reports have been published so far on the importance of residue 18 in membrane binding and membrane interactions using full-length hIAPP.

To shed light on the influence of residue 18 in membrane interactions, we have synthesized four mutated peptides where histidine 18 has been replaced by arginine (H18R-IAPP), lysine (H18K-IAPP), glutamic acid (H18E-IAPP) and alanine (H18A-IAPP) to achieve variations in charge, size and polarity. We determined the ability of the mutated peptides to insert into the membranes, to form fibrils at the membrane and to cause membrane damage. Our results demonstrate that the mutation at position 18 does not alter the ability of the peptide to insert into lipid bilayers. Furthermore the binding of all mutated peptides causes considerable damage to the membrane. However, the particular type of damage due to the mutated peptides is substantially different from that caused by native IAPP and is not related to fibril formation. The results obtained in our study suggest that the processes of IAPP-induced membrane damage and IAPP fibril growth at the membrane are highly sensitive to the residue at position 18.

2. Materials and methods

2.1. Peptide synthesis

All peptides were synthesized with a CEM Liberty Blue (CEM corporation, Matthews, USA) automated microwave peptide synthesizer using standard reaction cycles at the Institut de Biologie Intégrative (IFR83-Université Pierre et Marie Curie), as previously described [33]. The synthesis of the wild type and all the mutated peptides (Fig. 1), including an amidated C-terminus and a disulfide bridge, were performed using Fmoc chemistry and a PAL Novasyn TG resin. Two pseudoproline dipeptides were chosen for the synthesis: Fmoc-Ala-Thr (ΨMe,MePro)-OH replaced residues Ala-8 and Thr-9, and Fmoc-Leu-Ser (ΨMe,MePro)-OH replaced residues Leu-27 and Ser-28. Double couplings were performed for the pseudoprolines, for the residues following the pseudoprolines and for every β-branched residue. The peptides were cleaved from the resin and deprotected using standard TFA procedures with 1,2-ethanedithiol, water, and triisopropylsilane as scavengers. The peptides were purified by reverse phase high-

performance liquid chromatography (HPLC) with a Luna C18(2) column (Phenomenex, USA). A two-buffer system was used. Buffer A consisted of 100% H_2O and 0.1% TFA (vol/vol), and buffer B consisted of 100% acetonitrile and 0.07% TFA (v/v). Linear peptides were dissolved in aqueous DMSO (33%) and oxidized with air to the corresponding disulfide bond cyclic form. The purity of peptides was higher than 95% as determined by analytical HPLC and the identity of peptides was confirmed by MALDI-TOF mass spectrometry.

2.2. Peptide preparation

Peptide stock solutions were freshly prepared prior to all experiments using the same batch, as described previously [46]. Briefly, stock solutions were obtained by dissolving the peptide at a concentration of 1 mM in hexafluoroisopropanol (HFIP) and by leaving it to incubate for an hour. Then, HFIP was evaporated and the sample was dried by vacuum desiccation for at least 30 min. The resulting peptide film was dissolved at a concentration of 1 mM in DMSO for the fluorescence, microscopy and monolayers experiments (final DMSO concentration of 2.5% v/v) and then diluted in 50 mM Bis-Tris buffer, 100 mM NaCl (pH 7.4 or pH 5.5). For NMR experiments and CD experiments, no DMSO was used, the resulting peptide film was directly solubilized by addition of a dispersion of unilamellar vesicles in 50 mM phosphate buffer. Control experiments were performed to ensure that the use of these two different buffers did not affect the rate of fibril formation.

2.3. Preparation of phospholipid vesicles

Lipid films were made by dissolving the lipids in chloroform. The solvent was evaporated under dry nitrogen gas. The resulting films were then kept under vacuum desiccator for at least 30 min. Films were then rehydrated with appropriate buffer (50 mM Bis-Tris, 100 mM NaCl, for the Thioflavin experiments, TEM, and calcein leakage assay, and 50 mM sodium phosphate for NMR experiments) at a temperature above the transition temperature of the lipids for 30 min. The lipid suspensions were frozen in liquid nitrogen and thawed in a 40 °C water bath 3 times to obtain homogeneous multilamellar vesicles (MLVs). Unilamellar vesicles were prepared from the MLVs using the following protocol: the lipid suspensions were subjected to 10 freeze-thaw cycles, and passed 19 times through a mini-extruder (Avanti Polar Lipids, Alabaster, USA) equipped with a 200 nm polycarbonate membrane for Thioflavin experiments, TEM, and calcein leakage assay, and with a 50 nm polycarbonate membrane for NMR experiments. The phospholipid content of lipid stock solutions and vesicle preparations was quantified as inorganic phosphate according to Rouser [52]. Calcein-containing LUVs were made using the same protocol, except for the following adaptations: the buffer for hydration of the lipid films was replaced by a solution containing 70 mM calcein. Free calcein was separated from the calcein-filled LUVs using size-exclusion chromatography (Sephadex G50-fine) and elution with 100 mM Bis-Tris, 100 mM NaCl.

2.4. Monolayer experiments

Peptide-induced changes in the surface tension of a phospholipid monolayer were measured in a Langmuir trough using the DyneProbe (Kibron, Helsinki, Finland). Surface pressures were measured at room temperature. A trough was filled with 18 mL of freshly filtered 50 mM Tris.HCl buffer, 100 mM NaCl (pH 7.4). DOPC/DOPS (7:3) monolayers were spread from a 1 mM stock solution in chloroform. The lipid monolayer was allowed to stabilize for a few minutes before the addition of the peptide. The experiment was repeated five times, with different initial surface pressures ranging from 15 to 35 mN/m. The lipid monolayer was allowed to stabilize for a few minutes before 18 µL of a 1 mM stock solution of the peptide in DMSO was injected in the subphase without disturbing the lipid monolayer, resulting in a final peptide concentration of 1 µM. Higher peptide concentrations did not significantly increase the surface pressure.

2.5. CD spectroscopy

CD spectra were measured on a Jasco 815 spectropolarimeter (Jasco Inc., Easton, MD) over the wavelength range 190–260 nm, by using a 0.1 cm path length quartz cell (Hellma GmbH, Germany) with an internal volume of 200 µL. CD spectra were recorded at 25 °C, at 0.2 nm intervals and using a 20 nm min^{-1} scan speed. Each spectrum reported is the average of four scans. Measurements were carried out in 50 mM phosphate buffer containing 100 mM NaF at pH 7.4. Peptide concentrations were 25 µM in the presence of lipids (peptide:lipid ratio 1:10).

2.6. Fibril formation assay

The kinetics of IAPP fibril formation in the presence of lipid membranes was measured using the fluorescence intensity increase upon binding of the fluorescent probe Thioflavin T (ThT) to fibrils. A plate reader and a standard 96-well black microtiter plate were used (Fluostar Optima, BMG LabTech, Germany). The fluorescence was measured at room temperature from the top of the plate every 10 min with 440 nm excitation filter and 480 nm emission filter.

The ThT fluorescence assay was started by adding 10 µL of a 0.2 mM IAPP (10 µM peptide) to 190 µL of a mixture of 10 µM ThT, DOPC/DOPS vesicles (100 µM lipids; peptide:lipid ratio 1:10) and 50 mM Bis-Tris, 100 mM NaCl (pH 7.4 or pH 5.5). The microtiter plate was shaken for 10 s (600 rpm) directly after addition of all components, but not during the measurements. The assays were performed 3 times, each in triplicate, on different days, using different IAPP stock solutions. The replicates of each system showed consistent reproducibility.

2.7. Membrane permeability assay

A plate reader was used to perform membrane leakage experiments in standard 96-well transparent microtiter plates (Fluostar Optima, Bmg Labtech). Measurements were conducted on calcein-loaded DOPC/DOPS 7:3 LUVs. The peptides at 10 µM were added to a mixture of calcein-containing LUVs in 50 mM Bis-Tris, 100 mM NaCl, pH 7.4 or pH 5.5 (peptide:lipid ratio of 1:10). Directly after addition of all peptides, the microtiter plate was shaken for 10 s using the shaking function of the plate reader but not during the measurements. Fluorescence was measured from the bottom, every 10 min, using a 485 nm excitation filter and a 520 nm emission filter. The temperature was approximately 28 °C ± 3 °C. The maximum leakage at the end of each measurement was determined *via* addition of 1 µL of 10% Triton X-100 to a final concentration of 0.05% (v/v). The release of fluorescent dye was normalized according to the following equation:

$$L(t) = (F_t - F_0)/(F_{100} - F_0)$$

L(t) is the fraction of dye released (normalized membrane leakage), F_t is the measured fluorescence intensity, and F_0 and F_{100} are the fluorescence intensities at times $t = 0$, and after addition of Triton X-100, respectively. The calcein leakage experiment was performed 3 times, each in triplicate, on different days. The results presented here are the average of the different experiments, ± standard deviation.

2.8. Electron microscopy

TEM was performed at the “Institut de Biologie Paris Seine” (IBPS, Paris, France) at the University Pierre and Marie Curie. Aliquots (20 µL) of the samples used for ThT fluorescence assays were removed after 3 days of each kinetic experiments, blotted on a glow-discharged carbon coated 200 mesh copper grids for 2 min and then negatively stained with saturated uranyl acetate for 45 s. Grids were examined using a ZEISS 912 Omega electron microscope operating at 80 kV.

2.9. NMR spectroscopy

The peptide films were dissolved at a concentration of 50 μM in the presence of small unilamellar vesicles (peptide:lipid ratio 1:10) containing 50 mM phosphate buffer in D_2O (pH 7.4) and immediately transferred in a Shigemi tube of 5 mm diameter. Experiments were recorded at 25 °C on a Bruker AVANCE III NMR spectrometer operating at a ^1H frequency of 500 MHz, equipped with a TCI cryoprobe. One-dimensional spectra were acquired over 8192 points using a spectral width of 6010 Hz. For each spectrum, 512 scans were accumulated leading to an experiment time of about 15 min. An exponential window function with 1 Hz line broadening was applied to all ^1H spectra prior to Fourier transform. The evolution in time of the peptide signal intensity for each lipid system was followed by recording one dimensional ^1H spectra for ~ 24 h. Peptide ^1H resonances (in the aromatic region between 6.7 and 7.4 ppm, where no lipid signals are observed) were then integrated and these values are plotted as a function of time, leading to a sigmoidal curve, than can be fitted by a modified Richards eq. [53]:

$I = (I_i + a_i x) + \frac{(I_f + a_f x)}{1 + e^{k(t-t1/2)}}$ where I is peptide intensity obtained from 1D ^1H NMR integral, I_i and I_f are the initial and final ^1H NMR intensities, a_i and a_f are the slopes before and after the oligomerization phase, $t_{1/2}$ is the time where the ^1H NMR intensity decays to 50% of the maximum ^1H NMR signal and k the elongation rate. Since the analysis is done for the integrated intensity of peptide ^1H resonances between 6.7 and 7.4 ppm, results are therefore average values. All raw NMR experimental data have been processed using the TopSpin program (Bruker) and further analysed for the integration and the fit using the modified Richards equation with a home-written program based on R program.

3. Results

3.1. Design of mutated peptides to study the role of residue 18 in hIAPP-membrane interactions

It has been shown that residue 18 is important for modulating IAPP cytotoxicity and IAPP aggregation in solution [33], but it is not clear how this affects the interaction of IAPP with lipid bilayers. To address the contribution of residue 18, we studied human IAPP as well as IAPP variants in which His-18 was replaced by i) the positively charged residues, arginine and lysine, ii) the negatively charged amino acid, glutamic acid, and iii) the neutral residue alanine. These substitutions were chosen because those residues differ in shape, volume, charge and hydrophobicity. All these factors could influence hIAPP-membrane insertion and lead to different ways of hIAPP-membrane self-assembly and hIAPP-induced membrane disruption. All the experiments were performed in the presence of lipid membranes composed of DOPC/DOPS in a 7:3 M ratio. This composition was chosen because these phospholipids represent the most abundant zwitterionic phospholipid species (PC) and the dominant negatively charged phospholipid species (PS) in eukaryotic cells. The 7:3 ratio was chosen because it resembles the ratio of zwitterionic lipids to negatively charged lipids of the membrane of pancreatic islet cells [54].

3.2. Mutations at position 18 only slightly alter hIAPP-membrane insertion and hIAPP-membrane conformation

We first performed membrane surface pressure measurements on lipid monolayers to examine the ability of the peptides to insert into lipid membranes and to determine if residue 18 is important for membrane insertion. As shown in Fig. 1, injection of all peptides into the aqueous sub-phase below a lipid monolayer composed of DOPC/DOPS (7:3) results in a fast increase in the surface pressure, followed by a plateau after a few minutes (Fig. 2A). After 25 min, at an initial surface pressure of ~20 mN/m, the increase in surface pressure induced by

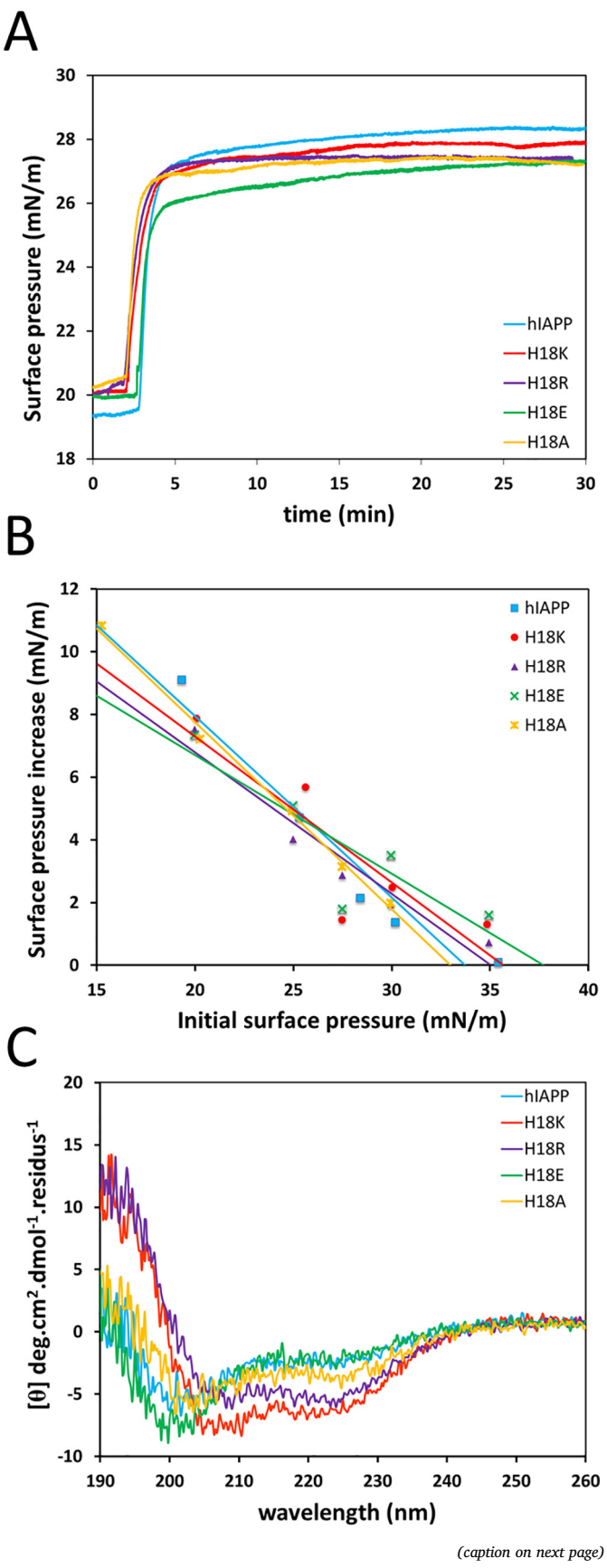

(caption on next page)

Fig. 2. Surface pressure profile (A) after injecting a sample of native hIAPP (blue), H18K-IAPP (red), H18R-IAPP (purple), H18E-IAPP (green) and H18A-IAPP (yellow) in a DOPC/DOPS monolayer (7:3). The peptides were injected into the stirred subphase at time zero. (B) Surface pressure increase induced by the interaction of freshly dissolved native hIAPP (blue), H18K-IAPP (red), H18R-IAPP (purple), H18E-IAPP (green) and H18A-IAPP (yellow) with DOPC/DOPS (7:3) monolayers as a function of the initial surface pressure. The straight lines were obtained by linear regression. Experimental error is estimated at ± 0.5 mN/m. (C) CD spectra of 25 μM native hIAPP (blue) and the mutative peptides (H18K, red; H18R, purple; H18E, green; H18A, yellow) freshly dissolved and added to DOPC/DOPS (7:3) vesicles 50 mM phosphate buffer containing 100 mM NaF. The absorbance values were expressed as mean residue molar ellipticity [θ].

insertion of native hIAPP is 9.0 mN/m, consistent with previous reports [55]. Using a similar initial surface pressure of ~20 mN/m, the insertion of all mutated peptides yields a slightly lower increase in surface pressure from 7.2 mN/m (H18A-IAPP), 7.4 mN/m (H18R-IAPP), 7.6 mN/m (H18E-IAPP) to 7.8 mN/m (H18K-IAPP), in all cases with an estimated experimental error of 0.5 mN/m. This result demonstrates that all peptides insert efficiently into lipid monolayers and that the mutations do not strongly influence the monolayer insertion within the experimental error range.

Next, in order to determine the maximum initial surface pressure enabling the peptides to insert, we monitored the surface pressure increase as function of the initial surface pressure (Fig. 2B). Our data indicate that the extrapolating maximum insertion pressure is high for all the peptides, ranging from ~33–38 mN/m. These limiting surface pressures are at least as high as the surface pressures that correspond to native biological membranes [56], indicating that *in vivo*, the peptides could insert efficiently into these membranes.

Fig. 2C displays the CD spectrum of the wild-type and the mutated peptides in the presence of DOPC/DOPS (7:3) membranes. Native hIAPP and the mutated peptides adopt a mixture of mostly random coil and α-helical structure, but with the highest α-helical content for H18R-IAPP and H18K-IAPP. These results show that the mutation somehow modulates the conformation that is adopted by the peptide upon addition to the vesicles.

3.3. Importance of residue 18 in self-assembly at the membrane surface

We previously showed that the mutated peptides form fibrils in solution but are less amyloidogenic than native hIAPP [33]. To investigate the importance of the residue 18 in hIAPP fibril formation at the membrane surface, fluorescence-detected thioflavin T binding assays, transmission electron microscopy (TEM) and ^{1}H NMR studies were conducted in the presence of unilamellar vesicles composed of DOPC and DOPS in a molar ratio of 7:3. First, we followed the kinetics of fibril formation by measuring the fluorescence intensity increase upon binding of the amyloid specific dye thioflavin T (ThT). Amyloid fibril formation follows a sigmoidal time course in which no detectable amyloid fibrils are formed during the lag phase. The lag phase is followed by a growth phase during which fibrils develop and elongate, eventually leading to a steady state where fibrils are in equilibrium with soluble peptide. As shown in Fig. 3A, a typical sigmoidal S-shaped curve was obtained for native hIAPP with a lag-time of approximately 4 h. Clear differences in the kinetics profile are observed for hIAPP and the analogs in terms of initial half-time $t_{1/2}$ and maximum intensity of the plateau, which give insight into the kinetics of the aggregation process and the amount of fibrillary material formed, respectively. Indeed, all of the mutated peptides show either a decreased amount of fibril formed, mostly in combination with an increased half-time, or they showed no fibril formation at all, indicating that the mutated peptides have a lower amyloidogenic propensity than native hIAPP in the presence of lipid membranes (Fig. 3B–C). H18K-IAPP shows the same half-time as native IAPP (around 4 h) but an important reduction in fluorescence plateau is observed (around 75%). An increase in the half-time and a reduction of the fluorescence intensity at the plateau are both observed for H18R-IAPP. Finally, H18A-IAPP and H18E-IAPP do not show significant fibril formation within 2 days of incubation.

In order to observe the early stages of the oligomerization process, namely during the lag phase of ThT fluorescence experiments, liquid state ^{1}H NMR spectra were recorded as described previously [53,57]. This allows us to observe the signal of the peptides over time in the monomeric state (or small oligomeric states such as dimers or trimers). As peptide self-assembly occurs, the intensities of peaks due to the monomer species decrease as a result of the conversion of the NMR-visible monomer to NMR-invisible large assemblies. Fig. 3D shows the aromatic region (between 6.7 and 7.4 ppm) of the signal of monomeric native hIAPP. The NMR spectra of hIAPP exhibit a sharp drop in intensity within the first hours, suggesting a rapid evolution of the monomer into oligomeric species which evolve into larger assemblies and protofibrils by nucleation and elongation-dependent pathway. ^{1}H NMR signals were fitted with a Richards function in order to obtain the rates of monomer depletion and estimate the fraction of residual monomer. The peptide ^{1}H signal decays to zero indicating that the monomeric peptide form in solution disappears completely. Experiments on the mutated peptides show clear differences in the kinetics of monomer depletion (Fig. 3E). The rate of monomer to large species evolution is slower for all the mutated peptides indicating that the monomeric species are more stable. It is also important to note that the normalized peak intensity does not decrease to zero for H18A-IAPP, H18K-IAPP and H18R-IAPP, suggesting that the monomer is still present after several hours of incubation. The time required to reach 50% of monomer depletion ($t_{1/2}$) is reported in Fig. 3F. Our data clearly indicate that native IAPP has the shortest $t_{1/2}$ compared to the mutated peptides. The H18E-IAPP analog shows the most divergent behavior as it remains mostly monomeric within the 22 h of NMR experiments, and only a small decrease of signal intensity can be observed at the end of incubation period. The results of NMR and fluorescence experiments showed that the rates of monomer depletion for the peptides were somewhat consistent with the rate of fibril formation. The NMR and ThT data indicate the following order of fibrillogenicity and monomer depletion: 18H > 18 K, 18R > 18A.

Consistent with the ThT fluorescence and NMR experiments, we observed using TEM the formation of typical long and twisted fibrils for native hIAPP and H18K-IAPP (Fig. 3G,H) after 4 days of incubation, while for H18R-IAPP only thin and small fibrils with a lower amount were observed (Fig. 3I) and almost no fibrils were detected after the same time of incubation for H18E-IAPP and H18A-IAPP (Fig. 3J,K).

3.4. Membrane disruption is controlled by residue 18

Then, the ability of the peptides to permeabilize large unilamellar vesicles was examined by measuring the fluorescence signal of the encapsulated fluorophore, calcein. The self-quenching dye, calcein, was entrapped at high concentration in DOPC/DOPS (7:3 M ratio) LUVs and incubated with either native IAPP or a mutated peptide. Upon addition of a membrane-damaging peptide, disruption of the lipid bilayer allows the escape of calcein, eliminating the self-quenching and resulting in an increase in the fluorescence signal. A time trace of dye leakage induced by the peptides is shown in Fig. 4. Our data indicate that native hIAPP induces significant leakage in DOPC/DOPS vesicles to about 60% of the total vesicle content. The process of hIAPP-induced membrane leakage is characterized by an S-shaped curve with a $t_{1/2}$ of approximately 7.5 h and an extent leakage of 60 ± 7%. In addition, membrane permeabilization induced by the peptides occurs in two distinct stages (Fig. 4). A rapid and near-exponential increase is observed, suggesting aspecific leakage process or transient pore formation at the membrane [58,59], followed by a second increase with a sigmoidal profile. The first event was already observed for antimicrobial peptides and both events were detected for amyloidogenic peptides [60–62]. Indeed, study on the aggregating amyloid β, Aβ40, involved in Alzheimer's disease, revealed a two-stage membrane damage mechanism, which was proposed to

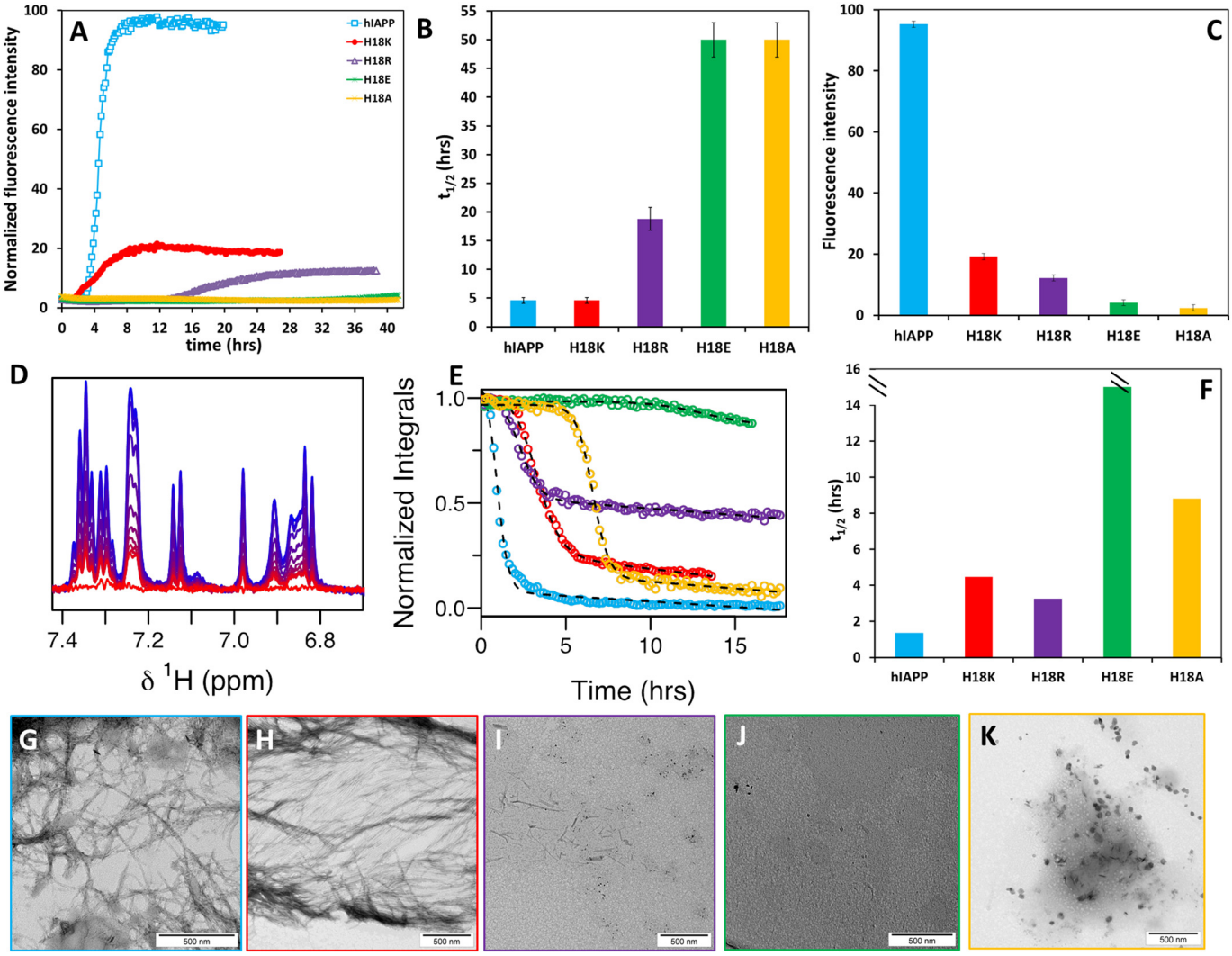

Fig. 3. (A) Kinetics of fibril formation for native hIAPP and the mutated IAPP (H18K, red; H18R, purple; H18E, green; and H18A, yellow) at 10 μM in the presence of DOPC/DOPS LUVs (pH 7.4). (B) Average midpoints (half-time $t_{1/2}$) of the sigmoidal transition for the different peptides. Since fibril elongation was not observed for H18E-IAPP and H18A-IAPP after 44 h of incubation, the $t_{1/2}$ could not be determined and only the lower limits are indicated (C) Fluorescence intensity of the plateau region for the different peptides. Average values and error bars were calculated using data of three independent measurements where each measurement provided three data points (*i.e.*, nine data points in total). (D) 1D ^{1}H NMR spectra (aromatic region) of native hIAPP at 50 μM observed over time in the presence of DOPC/DOPS SUVs (pH 7.4 in D_2O). Data shown correspond to spectra recorded every 15 min within the first 3 h (plot color code: from blue to red) and the final spectrum after 24 h. (E) NMR signal intensity of native hIAPP and the mutated IAPP (H18K, red; H18R, purple; H18E, green; and H18A, yellow) over time. (F) Average midpoints ($t_{1/2}$) of the sigmoidal transition observed by NMR for the different peptides. Kinetics of monomer depletion did not show a clear sigmoidal curve for H18E-IAPP, only lower limit of $t_{1/2}$ is shown on the graph. (G to K) TEM images of native hIAPP (G) and mutated IAPP (H18K, H; H18R, I; H18E, J; and H18A, K) in the presence of DOPC/DOPS vesicles. Scale bars represent 500 nm.

involve a primary selective pore formation followed by a non-selective membrane damage through fibril growth [62]. In addition, our data indicate that all mutations slow down the kinetics of membrane damage in the second stage compared to the native hIAPP. The extent of leakage in the second stage is roughly similar for all the mutated peptides (from 42% ± 6% to 52% ± 6% of the total vesicles content measured after 24 h). Together with the ThT, TEM and NMR experiments, these results strongly suggest that the mutated peptides H18R-IAPP, H18E-IAPP and H18A-IAPP lead to significant membrane damage but that the membrane leakage is not related to fibril formation.

3.5. Detection of high oligomeric species at low pH

To slow down the fibril formation and the membrane leakage and be able to dissect the first events of membrane damage, we performed calcein-leakage experiments and we recorded TEM images at pH 5.5. Previous studies in solution reported that the kinetics of fibril formation is retarded at pH 5.5 compared to pH 7.4 for native hIAPP [63] and for the hIAPP analogs [33]. Our ThT results are consistent with these studies and show that in the presence of lipid membranes, low pH slows down IAPP fibril formation for the wild-type peptide as well as for the H18K-IAPP and H18R-IAPP (Fig. 5A). However under this acidic condition, the peptides are still able to damage membrane. Fig. 5B shows that in DOPC/DOPS vesicles at 10 μM peptide native hIAPP and H18K-IAPP induce ~60% and ~50% of membrane leakage, respectively, after incubation for 40 h, while H18R-IAPP, H18A-IAPP and H18E-IAPP slightly permeabilize lipid vesicles (between 20% and 30%). We also observed at pH 5.5 an initial leakage stage within the first 3 h suggesting oligomeric pore formation or aspecific leakage.

Finally, TEM was used to visualize the potential interaction between the peptides and the lipid membrane and to investigate which IAPP species interact with the membranes. Fig. 5C shows that after incubating hIAPP three days with the lipid vesicles, hIAPP fibrils are formed that line the surface of the vesicles (asterisks in Fig. 5C). The size and the morphology of these fibrils are similar to those of hIAPP fibrils formed in the absence of vesicles [33]. It is interesting to note

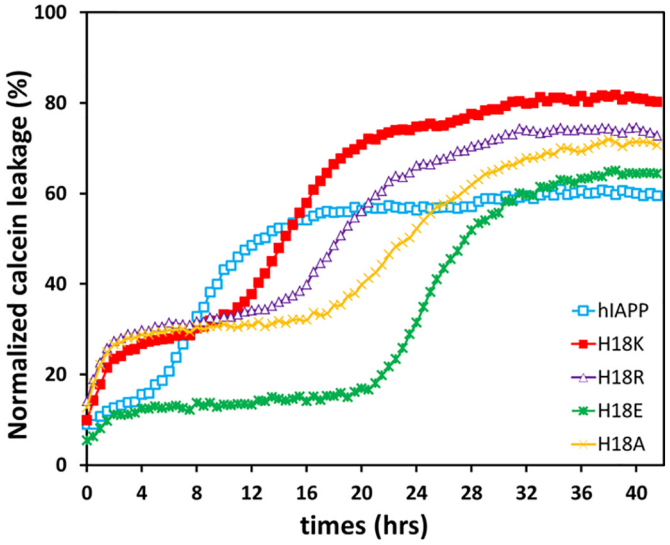

Fig. 4. Kinetics of membrane permeabilization induced by 10 μM native hIAPP (blue), H18K-IAPP (red), H18R-IAPP (purple), H18E-IAPP (green) and H18A-IAPP (yellow). The peptides were added to the calcein-containing DOPC/DOPS (7:3) LUVs at time zero.

that most of the vesicles in contact with hIAPP fibrils are distorted, showing noncircular shapes. The distortion of the vesicles was previously observed and related to hIAPP fibril formation at the surface of the vesicles [31]. Different behavior is observed for the mutated peptides (Fig. 5D–G). For H18K-IAPP, we observed a very large dense network with thick fibrils. Rare vesicles could be seen in between the network of H18K-IAPP fibrils (asterisk in Fig. 5D). For H18E-IAPP, H18A-IAPP and H18R-IAPP, small amounts of thin material together with some amorphous structures but no amyloid fibrils were detected at pH 5.5. However, it is the specific localization of those structure that is perhaps most noteworthy. Indeed, most of the amorphous and small structures are observed along the surface of the membranes. We also found the appearance of defects or pores in the membrane induced by H18A-IAPP and H18R-IAPP, indicating that the membrane leakage induced by H18A-IAPP and H18R-IAPP is probably due to the formation of large oligomeric species but not to the fibril growth. H18E-IAPP also induces membrane defects, probably through formation of oligomers, but these defects are probably too small to be detected by TEM.

4. Discussion

Full length IAPP peptide can be divided into two regions: the N-terminal part from residues 1 to 19 which determines the membrane binding and the 20–37 segment, which constitutes the spine of amyloid fibrils and is essential for its formation [31,38,64,65]. The non amyloidogenic and nontoxic mouse IAPP differs from human IAPP by six residues out of 37, only one residue being in the membrane binding 1–19 region. Understanding the conditions that result in membrane disruption by hIAPP can be essential in developing strategies to prevent amyloidosis in T2DM. Thus, the goal of our work is to provide insight into the interaction between mature IAPP and lipid membranes and to dissect the mechanism of membrane disruption. In order to do so, we investigated the role of residue 18, the sole residue in the membrane interacting domain which differs with the non-amyloidogenic mouse IAPP, using four mutated peptides. In particular, we examined IAPP-membrane interaction at three different levels: i) membrane insertion, ii) IAPP fibril formation at the membrane surface and iii) membrane-disruption induced by IAPP oligomerization or by IAPP fibril formation. Our results show that the mutation at the residue 18 has a pronounced effect on IAPP fibril formation and on IAPP membrane damage but not

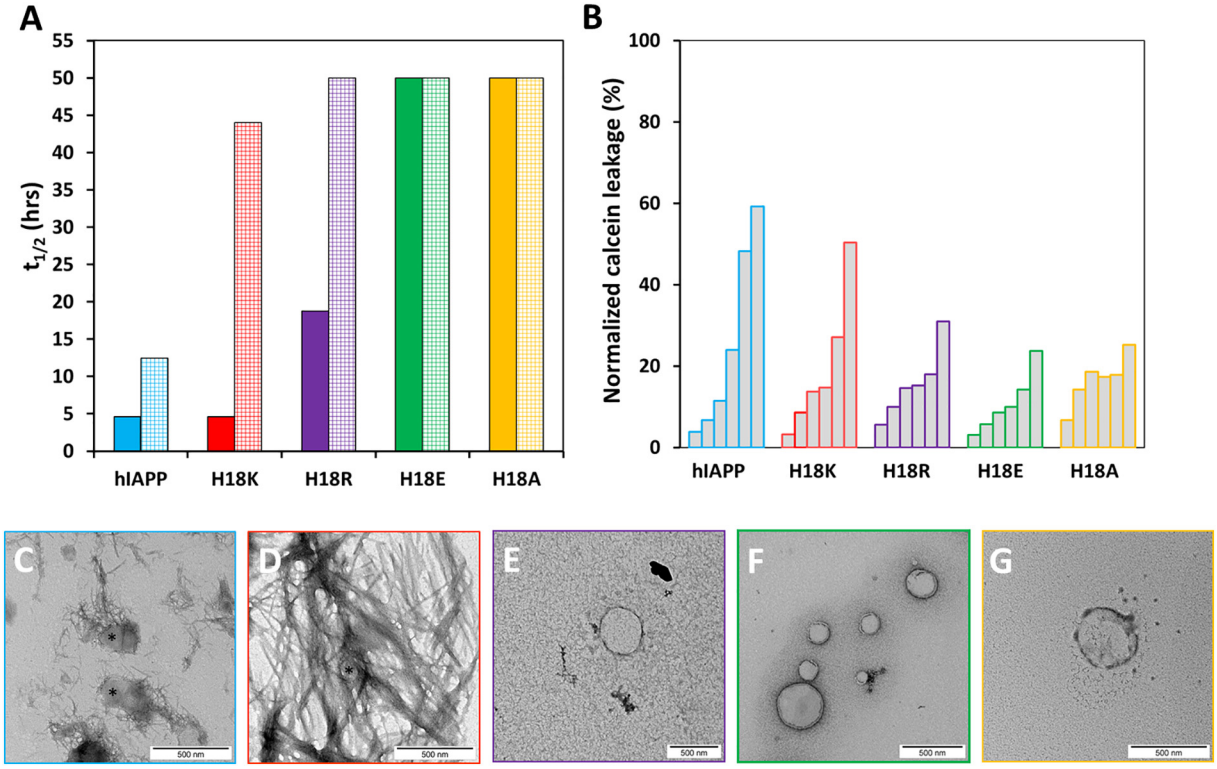

Fig. 5. (A) Calculated half-time ($t_{1/2}$) of native IAPP and mutated IAPP fibril formation in the presence of DOPC/DOPS vesicles (H18K, red; H18R, purple; H18E, green; H18A, yellow) at pH 7.4 (plain bars) and pH 5.5 (dashed bars). Since fibril elongation was not always observed for the mutated peptides after 45 h of incubation, the $t_{1/2}$ could not be determined and only the lower limits are indicated (B) Membrane damage induced by 10 μM native IAPP and mutated peptides after prolonged incubation with calcein-loaded LUVs at pH 5.5. Vesicle leakage was determined after incubation of LUVs for 1 min, 3 h, 10 h, 20 h, 30 h and 40 h with peptides. (C to G) TEM images of native hIAPP (C) and mutated IAPP in the presence of DOPC/DOPS vesicles after three days of incubation (H18K, D; H18R, E; H18E, F; and H18A, G) at pH 5.5. Scale bars represent 500 nm.

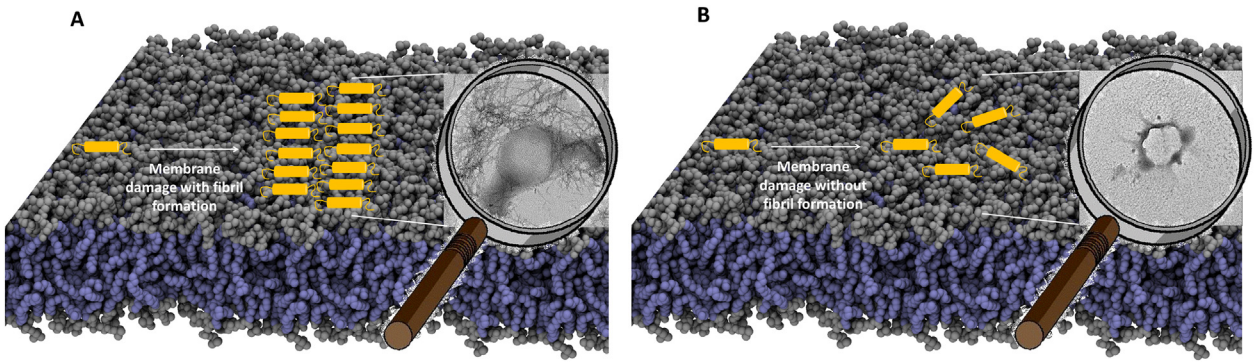

Fig. 6. Proposed models for membrane insertion, oligomerization and membrane disruption by native hIAPP and H18K-IAPP (A) and by H18R-IAPP, H18E-IAPP and H18A-IAPP (B) based on monolayer, fluorescence, NMR and microscopy experiments. Before binding to the membrane, hIAPP exists primarily as a monomeric (or weakly oligomerized) species. The peptides insert into the membrane *via* their N-terminal part. Wild type IAPP and H18K-IAPP rapidly form stable fibrils leading to membrane disruption (Fig. 6A). On the other hand H18E-IAPP, H18A-IAPP and H18R-IAPP do not aggregate into amyloid fibrils (Fig. 6B). The membrane leakage could be due in this case to the accumulation of high molecular weight aggregates at the surface, as observed in TEM images.

on IAPP membrane insertion. These findings are discussed below, together with a proposed model (Fig. 6).

It was reported that the electrostatic interactions between the positively charged residues and negatively charged lipids are important for peptide-membrane association [37,66]. Our data demonstrate that all the mutated peptides insert into the lipid membrane suggesting that the charge is not the sole factor controlling the membrane binding behavior. Indeed, IAPP will also probably interact with lipid chains *via* hydrophobic interactions. The monolayer and fluorescence data reveal that membrane insertion is not sufficient to cause IAPP amyloid aggregation. All the peptides bind to the membrane but only two of them aggregate rapidly into amyloid fibrils, native IAPP and H18K-IAPP. The fluorescence experiments together with the microscopy clearly show that the time course and the quantity of fibril formation are strongly dependent on residue 18. ThT fluorescence experiments demonstrated that both H18E-IAPP and H18A-IAPP do not form fibrils within a few days of incubation and NMR experiments indicated that > 80% signal of monomeric H18E-IAPP is still present after 20 h of incubation. Our results also indicate that the histidine to arginine substitution largely decreases IAPP fibril formation and approximately 50% signal of monomeric H18R-IAPP is observed after 24 h of incubation. These results suggest that monomeric and small oligomeric H18E-IAPP, H18R-IAPP and H18A-IAPP do not disappear completely and that the substitution of the histidine by an arginine, an alanine or a glutamic acid stabilizes the monomeric or small oligomeric species.

It is clear that hIAPP can induce membrane damage which is believed to be one of the causes of β cell death [15,16]. Previous reports, based on cell toxicity on INS 1 cells, a pancreatic cell line commonly used in studies of IAPP toxicity, revealed that all mutated peptides induce less toxicity than wild type hIAPP [33]. Nevertheless our leakage experiments *in vitro* indicate a similar extent of final membrane leakage for native hIAPP and the mutated peptides, albeit with very different kinetics. We suggest that IAPP cytotoxicity is not directly linked to the extent of membrane damage *in vitro* but rather to the kinetics of this process. Furthermore, cell membrane perturbation, although evidenced *in vivo* [15,16,19,67], is probably not the only mechanism contributing to the cytotoxicity.

The mechanism of hIAPP-induced membrane disruption is not completely understood. Several mechanisms have been proposed to explain hIAPP induced membrane damage. Some studies described a mechanism *via* non-specific pores or ion-channel [16,29,30,68] while other studies proposed that hIAPP acts like a detergent and disturbs the membrane integrity *via* carpeting mechanisms [69]. Finally, it was also shown that the growth of hIAPP fibrils at the membrane surface lead to membrane alterations such as disruption or fragmentation, which could lead to partial removal of the lipids from the membrane interface [19,31,32,70,71]. Consistent with these different reports, the biphasic nature of the leakage profile, which is observed for both native and mutated peptides, could correspond to distinct mechanisms and involved species. The first leakage stage occurs rapidly for all the peptides without any detectable lag phase. This step does not appear to be linked to an increase in ThT fluorescence, neither to a significant consumption of monomer as seen by NMR, suggesting that it is not due to the fibril growth but probably to the rapid binding to the surface of monomers or weakly oligomerized species.

Our data suggest different mechanisms for the second stage of membrane damage depending of the residue 18, which are schematically depicted in Fig. 6. For wild type IAPP and H18K-IAPP, the kinetics profile of membrane permeabilization follows that of fibril formation. As proposed before for wild type hIAPP, the membrane disruption induced by H18K-IAPP appears right after the fibril formation suggesting that small oligomers are not involved in the loss of the barrier function, but that the fibril formation at the membrane surface leads to membrane damage.

In contrast, fibrils could not be detected by ThT fluorescence for H18E-IAPP and H18A-IAPP and only marginally for H18R-IAPP. This suggests that fibril growth is not involved in membrane damage for these three IAPP mutants. The existence of a lag-time in the second leakage stage can be explained by the slow buildup of large species that are not directly visible by ThT-fluorescence but can be inferred indirectly from NMR experiments revealing a significant consumption of the monomer. The TEM images at pH 5.5 display some aggregates around the membrane interface and an important membrane alteration can be seen especially with H18A-IAPP (Fig. 5G). We thus propose that it is the accumulation of high molecular weight oligomeric species at the membrane surface, but not fibrils, which promotes a membrane leakage in the case of H18E-IAPP, H18A-IAPP or H18R-IAPP. Residue 18 turns out to have an important effect not only on the kinetics and the amount of fibrils formed at the membrane but also on the mechanism of membrane leakage. In particular, for the mutated peptides that are severely impacted in their ability to form fibrils, the membrane leakage would involve large aggregated species distinct from fibrils.

The following is the supplementary data related to this article.

Fig. SI-1 1D ^{1}H NMR spectra (aromatic region) of native hIAPP and the four mutants (50 μM concentration) observed over time in the presence of DOPC/DOPS SUVs (pH 7.4 in D_2O). Data shown correspond to spectra recorded every 15 min within the first 3 h (plot color code: from blue to green) and then spectra recorded every 2.5 h up to 1 day (from orange to red).

Transparency document

The http://dx.doi.org/10.1016/j.bbamem.2018.02.018 associated with this article can be found, in online version.

Acknowledgements

Christophe Piesse (Institut de Biologie Paris Seine, Université Pierre et Marie Curie, France) is acknowledged for the peptides synthesis. We thank Michael Trichet (Institut de Biologie Paris Seine, Université Pierre et Marie Curie, France) for valuable discussions on electron microscopy. We are deeply grateful to Patrick Fuchs (Université Paris Diderot, France) for the phospholipid membrane snapshots.

Appendix A. Supplementary data

Supplementary data to this article can be found online at https://doi.org/10.1016/j.bbamem.2018.02.018.

References

[1] F. Chiti, C.M. Dobson, Protein misfolding, functional amyloid, and human disease, Annu. Rev. Biochem. 75 (2006) 333–366.
[2] J.W.M. Höppener, B. Ahrén, C.J.M. Lips, Islet amyloid and type 2 diabetes mellitus, N. Engl. J. Med. 343 (2000) 411–419.
[3] G.J. Cooper, A.C. Willis, A. Clark, R.C. Turner, R.B. Sim, K.B. Reid, Purification and characterization of a peptide from amyloid-rich pancreases of type 2 diabetic patients, Proc. Natl. Acad. Sci. U. S. A. 84 (1987) 8628–8632.
[4] P. Westermark, C. Wernstedt, E. Wilander, D.W. Hayden, T.D. O'Brien, K.H. Johnson, Amyloid fibrils in human insulinoma and islets of Langerhans of the diabetic cat are derived from a neuropeptide-like protein also present in normal islet cells, Proc. Natl. Acad. Sci. 84 (1987) 3881–3885.
[5] G.T. Westermark, P. Westermark, C. Berne, O. Korsgren, Nordic network for clinical islet transplantation, widespread amyloid deposition in transplanted human pancreatic islets, N. Engl. J. Med. 359 (2008) 977–979.
[6] J. Udayasankar, K. Kodama, R.L. Hull, S. Zraika, K. Aston-Mourney, S.L. Subramanian, J. Tong, M.V. Faulenbach, J. Vidal, S.E. Kahn, Amyloid formation results in recurrence of hyperglycaemia following transplantation of human IAPP transgenic mouse islets, Diabetologia 52 (2009) 145–153.
[7] B. Konarkowska, J.F. Aitken, J. Kistler, S. Zhang, G.J.S. Cooper, The aggregation potential of human amylin determines its cytotoxicity towards islet beta-cells, FEBS J. 273 (2006) 3614–3624.
[8] C.A. Jurgens, M.N. Toukatly, C.L. Fligner, J. Udayasankar, S.L. Subramanian, S. Zraika, K. Aston-Mourney, D.B. Carr, P. Westermark, G.T. Westermark, S.E. Kahn, R.L. Hull, β-cell loss and β-cell apoptosis in human type 2 diabetes are related to islet amyloid deposition, Am. J. Pathol. 178 (2011) 2632–2640.
[9] K.J. Potter, A. Abedini, P. Marek, A.M. Klimek, S. Butterworth, M. Driscoll, R. Baker, M.R. Nilsson, G.L. Warnock, J. Oberholzer, S. Bertera, M. Trucco, G.S. Korbutt, P.E. Fraser, D.P. Raleigh, C.B. Verchere, Islet amyloid deposition limits the viability of human islet grafts but not porcine islet grafts, Proc. Natl. Acad. Sci. 107 (2010) 4305–4310.
[10] M. Stumvoll, B.J. Goldstein, T.W. van Haeften, Pathogenesis of type 2 diabetes, Endocr. Res. 32 (2007) 19–37.
[11] A. Lorenzo, B. Razzaboni, G.C. Weir, B.A. Yankner, Pancreatic islet cell toxicity of amylin associated with type-2 diabetes mellitus, Nature 368 (1994) 756–760.
[12] D.L. Hay, G. Christopoulos, A. Christopoulos, P.M. Sexton, Amylin receptors: molecular composition and pharmacology, Biochem. Soc. Trans. 32 (2004) 865–867.
[13] D.S. Wimalasena, B.E. Janowiak, S. Lovell, M. Miyagi, J. Sun, H. Zhou, J. Hajduch, C. Pooput, K.L. Kirk, K.P. Battaile, J.G. Bann, Evidence that histidine protonation of receptor-bound anthrax protective antigen is a trigger for pore formation, Biochemistry 49 (2010) 6973–6983.
[14] T.A. Lutz, Control of energy homeostasis by amylin, Cell. Mol. Life Sci. 69 (2012) 1947–1965.
[15] J. Janson, R.H. Ashley, D. Harrison, S. McIntyre, P.C. Butler, The mechanism of islet amyloid polypeptide toxicity is membrane disruption by intermediate-sized toxic amyloid particles, Diabetes 48 (1999) 491–498.
[16] T.A. Mirzabekov, M.C. Lin, B.L. Kagan, Pore formation by the cytotoxic islet amyloid peptide amylin, J. Biol. Chem. 271 (1996) 1988–1992.
[17] J.A. Hebda, A.D. Miranker, The interplay of catalysis and toxicity by amyloid intermediates on lipid bilayers: insights from type II diabetes, Annu. Rev. Biophys. 38 (2009) 125–152.
[18] X. Zhang, E. London, D.P. Raleigh, Sterol structure strongly modulates membrane-IAPP interactions, Biochemistry (2018).
[19] P. Cao, A. Abedini, H. Wang, L.-H. Tu, X. Zhang, A.M. Schmidt, D.P. Raleigh, Islet amyloid polypeptide toxicity and membrane interactions, Proc. Natl. Acad. Sci. 110 (2013) 19279–19284.
[20] A. Martel, L. Antony, Y. Gerelli, L. Porcar, A. Fluitt, K. Hoffmann, I. Kiesel, M. Vivaudou, G. Fragneto, J.J. de Pablo, Membrane permeation versus amyloidogenicity: a multitechnique study of islet amyloid polypeptide interaction with model membranes, J. Am. Chem. Soc. 139 (2017) 137–148.
[21] J. Hardy, The amyloid hypothesis of Alzheimer's disease: progress and problems on the road to therapeutics, Science 297 (2002) 353–356.
[22] B. Caughey, P.T. Lansbury, Protofibrils, pores, fibrils and neurodegenertion: separating the responsible protein aggregates from the innocent bystanders, Annu. Rev. Neurosci. 26 (2003) 267–298.
[23] G.B. Irvine, O.M. El-Agnaf, G.M. Shankar, D.M. Walsh, Protein aggregation in the brain: the molecular basis for Alzheimer's and Parkinson's diseases, Mol. Med. Camb. Mass 14 (2008) 451–464.
[24] R. Kayed, Common structure of soluble amyloid oligomers implies common mechanism of pathogenesis, Science 300 (2003) 486–489.
[25] Y. Suzuki, J.R. Brender, K. Hartman, A. Ramamoorthy, E.N.G. Marsh, Alternative pathways of human islet amyloid polypeptide aggregation distinguished by ^{19}F nuclear magnetic resonance-detected kinetics of monomer consumption, Biochemistry 51 (2012) 8154–8162.
[26] S.M. Vaiana, R. Ghirlando, W.-M. Yau, W.A. Eaton, J. Hofrichter, Sedimentation studies on human amylin fail to detect low-molecular-weight oligomers, Biophys. J. 94 (2008) L45–L47.
[27] R. Soong, J.R. Brender, P.M. Macdonald, A. Ramamoorthy, Association of Highly compact type II diabetes related islet amyloid polypeptide intermediate species at physiological temperature revealed by diffusion NMR spectroscopy, J. Am. Chem. Soc. 131 (2009) 7079–7085.
[28] H.-L. Zhao, Y. Sui, J. Guan, L. He, X.-M. Gu, H.K. Wong, L. Baum, F.M.M. Lai, P.C.Y. Tong, J.C.N. Chan, Amyloid oligomers in diabetic and nondiabetic human pancreas, Transl. Res. 153 (2009) 24–32.
[29] M. Anguiano, R.J. Nowak, P.T. Lansbury, Protofibrillar islet amyloid polypeptide permeabilizes synthetic vesicles by a pore-like mechanism that may be relevant to type II diabetes, Biochemistry 41 (2002) 11338–11343.
[30] A. Quist, I. Doudevski, H. Lin, R. Azimova, D. Ng, B. Frangione, B. Kagan, J. Ghiso, R. Lal, Amyloid ion channels: a common structural link for protein-misfolding disease, Proc. Natl. Acad. Sci. 102 (2005) 10427–10432.
[31] M.F.M. Engel, L. Khemtemourian, C.C. Kleijer, H.J.D. Meeldijk, J. Jacobs, A.J. Verkleij, B. de Kruijff, J.A. Killian, J.W.M. Hoppener, Membrane damage by human islet amyloid polypeptide through fibril growth at the membrane, Proc. Natl. Acad. Sci. 105 (2008) 6033–6038.
[32] E. Sparr, M.F.M. Engel, D.V. Sakharov, M. Sprong, J. Jacobs, B. de Kruijff, J.W.M. Höppener, J. Antoinette Killian, Islet amyloid polypeptide-induced membrane leakage involves uptake of lipids by forming amyloid fibers, FEBS Lett. 577 (2004) 117–120.
[33] L. Khemtemourian, G. Guillemain, F. Foufelle, J.A. Killian, Residue specific effects of human islet polypeptide amyloid on self-assembly and on cell toxicity, Biochimie 142 (2017) 22–30.
[34] L. Caillon, A.R.F. Hoffmann, A. Botz, L. Khemtemourian, Molecular structure, membrane interactions, and toxicity of the islet amyloid polypeptide in type 2 diabetes mellitus, J. Diabetes Res. 2016 (2016) 1–13.
[35] A.N. Roberts, B. Leighton, J.A. Todd, D. Cockburn, P.N. Schofield, R. Sutton, S. Holt, Y. Boyd, A.J. Day, E.A. Foot, Molecular and functional characterization of amylin, a peptide associated with type 2 diabetes mellitus, Proc. Natl. Acad. Sci. U. S. A. 86 (1989) 9662–9666.
[36] R. Akter, P. Cao, H. Noor, Z. Ridgway, L.-H. Tu, H. Wang, A.G. Wong, X. Zhang, A. Abedini, A.M. Schmidt, D.P. Raleigh, Islet amyloid polypeptide: structure, function, and pathophysiology, J. Diabetes Res. 2016 (2016) 1–18.
[37] M.F.M. Engel, H. Yigittop, R.C. Elgersma, D.T.S. Rijkers, R.M.J. Liskamp, B. de Kruijff, J.W.M. Höppener, J. Antoinette Killian, Islet amyloid polypeptide inserts into phospholipid monolayers as monomer, J. Mol. Biol. 356 (2006) 783–789.
[38] D.H.J. Lopes, A. Meister, A. Gohlke, A. Hauser, A. Blume, R. Winter, Mechanism of islet amyloid polypeptide fibrillation at lipid interfaces studied by infrared reflection absorption spectroscopy, Biophys. J. 93 (2007) 3132–3141.
[39] S.A. Jayasinghe, R. Langen, Lipid membranes modulate the structure of islet amyloid polypeptide, Biochemistry 44 (2005) 12113–12119.
[40] L. Caillon, O. Lequin, L. Khemtémourian, Evaluation of membrane models and their composition for islet amyloid polypeptide-membrane aggregation, Biochim. Biophys. Acta Biomembr. 1828 (2013) 2091–2098.
[41] M. Apostolidou, S.A. Jayasinghe, R. Langen, Structure of α-helical membrane-bound human islet amyloid polypeptide and its implications for membrane-mediated misfolding, J. Biol. Chem. 283 (2008) 17205–17210.
[42] S.M. Patil, S. Xu, S.R. Sheftic, A.T. Alexandrescu, Dynamic α-helix structure of micelle-bound human amylin, J. Biol. Chem. 284 (2009) 11982–11991.
[43] R.P.R. Nanga, J.R. Brender, S. Vivekanandan, A. Ramamoorthy, Structure and membrane orientation of IAPP in its natively amidated form at physiological pH in a membrane environment, Biochim. Biophys. Acta Biomembr. 1808 (2011) 2337–2342.
[44] G.L. Dignon, G.H. Zerze, J. Mittal, Interplay between membrane composition and structural stability of membrane-bound hIAPP, J. Phys. Chem. B 121 (2017) 8661–8668.
[45] D.C. Rodriguez Camargo, K.J. Korshavn, A. Jussupow, K. Raltchev, D. Goricanec, M. Fleisch, R. Sarkar, K. Xue, M. Aichler, G. Mettenleiter, A.K. Walch, C. Camilloni, F. Hagn, B. Reif, A. Ramamoorthy, Stabilization and structural analysis of a membrane-associated hIAPP aggregation intermediate, elife 6 (2017).
[46] L. Khemtémourian, M.F.M. Engel, R.M.J. Liskamp, J.W.M. Höppener, J.A. Killian, The N-terminal fragment of human islet amyloid polypeptide is non-fibrillogenic in the presence of membranes and does not cause leakage of bilayers of physiologically relevant lipid composition, Biochim. Biophys. Acta Biomembr. 1798 (2010) 1805–1811.
[47] K.K. Skeby, O.J. Andersen, T.V. Pogorelov, E. Tajkhorshid, B. Schiøtt, Conformational dynamics of the human islet amyloid polypeptide in a membrane environment: toward the aggregation prone form, Biochemistry 55 (2016) 2031–2042.
[48] J.R. Brender, E.L. Lee, M.A. Cavitt, A. Gafni, D.G. Steel, A. Ramamoorthy, Amyloid fiber formation and membrane disruption are separate processes localized in two distinct regions of IAPP, the type-2-diabetes-related peptide, J. Am. Chem. Soc. 130 (2008) 6424–6429.
[49] J.R. Brender, K. Hartman, K.R. Reid, R.T. Kennedy, A. Ramamoorthy, A single

mutation in the nonamyloidogenic region of islet amyloid polypeptide greatly reduces toxicity, Biochemistry 47 (2008) 12680–12688.
[50] J.R. Brender, J. Krishnamoorthy, G.M.L. Messina, A. Deb, S. Vivekanandan, C. La Rosa, J.E. Penner-Hahn, A. Ramamoorthy, Zinc stabilization of prefibrillar oligomers of human islet amyloid polypeptide, Chem. Commun. 49 (2013) 3339.
[51] S. Salamekh, J.R. Brender, S.-J. Hyung, R.P.R. Nanga, S. Vivekanandan, B.T. Ruotolo, A. Ramamoorthy, A two-site mechanism for the inhibition of IAPP amyloidogenesis by zinc, J. Mol. Biol. 410 (2011) 294–306.
[52] G. Rouser, S. Fkeischer, A. Yamamoto, Two dimensional then layer chromatographic separation of polar lipids and determination of phospholipids by phosphorus analysis of spots, Lipids 5 (1970) 494–496.
[53] L. Caillon, L. Duma, O. Lequin, L. Khemtemourian, Cholesterol modulates the interaction of the islet amyloid polypeptide with membranes, Mol. Membr. Biol. 31 (2014) 239–249.
[54] I. Rustenbeck, A. Matthies, S. Lenzen, Lipid composition of glucose-stimulated pancreatic islets and insulin-secreting tumor cells, Lipids 29 (1994) 685–692.
[55] L. Khemtémourian, G. Lahoz Casarramona, D.P.L. Suylen, T.M. Hackeng, J.D. Meeldijk, B. de Kruijff, J.W.M. Höppener, J.A. Killian, Impaired processing of human pro-islet amyloid polypeptide is not a causative factor for fibril formation or membrane damage in vitro, Biochemistry 48 (2009) 10918–10925.
[56] R.A. Demel, W.S. Geurts van Kessel, R.F. Zwaal, B. Roelofsen, L.L. van Deenen, Relation between various phospholipase actions on human red cell membranes and the interfacial phospholipid pressure in monolayers, Biochim. Biophys. Acta 406 (1975) 97–107.
[57] B.N. Ratha, A. Ghosh, J.R. Brender, N. Gayen, H. Ilyas, C. Neeraja, K.P. Das, A.K. Mandal, A. Bhunia, Inhibition of insulin amyloid fibrillation by a novel amphipathic heptapeptide: mechanistic details studied by spectroscopy in combination with microscopy, J. Biol. Chem. 291 (2016) 23545–23556.
[58] S. Rex, G. Schwarz, Quantitative studies on the melittin-induced leakage mechanism of lipid vesicles, Biochemistry 37 (1998) 2336–2345.
[59] G. Schwarz, C.H. Robert, Kinetics of pore-mediated release of marker molecules from liposomes or cells, Biophys. Chem. 42 (1992) 291–296.
[60] L. Caillon, J.A. Killian, O. Lequin, L. Khemtémourian, Biophysical investigation of the membrane-disrupting mechanism of the antimicrobial and amyloid-like peptide dermaseptin S9, PLoS One 8 (2013) e75528.
[61] J.R. Brender, E.L. Lee, K. Hartman, P.T. Wong, A. Ramamoorthy, D.G. Steel, A. Gafni, Biphasic effects of insulin on islet amyloid polypeptide membrane disruption, Biophys. J. 100 (2011) 685–692.
[62] M.F.M. Sciacca, S.A. Kotler, J.R. Brender, J. Chen, D. Lee, A. Ramamoorthy, Two-step mechanism of membrane disruption by Aβ through membrane fragmentation and pore formation, Biophys. J. 103 (2012) 702–710.
[63] L. Khemtémourian, E. Doménech, J.P.F. Doux, M.C. Koorengevel, J.A. Killian, Low pH acts as inhibitor of membrane damage induced by human islet amyloid polypeptide, J. Am. Chem. Soc. 133 (2011) 15598–15604.
[64] C. Goldsbury, K. Goldie, J. Pellaud, J. Seelig, P. Frey, S.A. Müller, J. Kistler, G.J.S. Cooper, U. Aebi, Amyloid fibril formation from full-length and fragments of amylin, J. Struct. Biol. 130 (2000) 352–362.
[65] E.T.A. Jaikaran, C.E. Higham, L.C. Serpell, J. Zurdo, M. Gross, A. Clark, P.E. Fraser, Identification of a novel human islet amyloid polypeptide β-sheet domain and factors influencing fibrillogenesis, J. Mol. Biol. 308 (2001) 515–525.
[66] X. Zhang, J.R. St, E. London Clair, D.P. Raleigh, Islet amyloid polypeptide membrane interactions: effects of membrane composition, Biochemistry 56 (2017) 376–390.
[67] A. Demuro, E. Mina, R. Kayed, S.C. Milton, I. Parker, C.G. Glabe, Calcium dysregulation and membrane disruption as a ubiquitous neurotoxic mechanism of soluble amyloid oligomers, J. Biol. Chem. 280 (2005) 17294–17300.
[68] N.B. Last, E. Rhoades, A.D. Miranker, Islet amyloid polypeptide demonstrates a persistent capacity to disrupt membrane integrity, Proc. Natl. Acad. Sci. 108 (2011) 9460–9465.
[69] J.D. Green, C. Goldsbury, J. Kistler, G.J.S. Cooper, U. Aebi, Human amylin oligomer growth and fibril elongation define two distinct phases in amyloid formation, J. Biol. Chem. 279 (2004) 12206–12212.
[70] J.R. Brender, S. Salamekh, A. Ramamoorthy, Membrane disruption and early events in the aggregation of the diabetes related peptide IAPP from a molecular perspective, Acc. Chem. Res. 45 (2012) 454–462.
[71] A. Junghans, E.B. Watkins, J. Majewski, A. Miranker, I. Stroe, Influence of the human and rat islet amyloid polypeptides on structure of phospholipid bilayers: neutron reflectometry and fluorescence microscopy studies, Langmuir 32 (2016) 4382–4391.